Performance Analysis and Optimization of a Solar Driven R134a Ejector Refrigeration System

Nkosinathi Shongwe [1], Aggrey Mwesigye [2], Hamed Roohani[1]

[1]School of Mechanical, Industrial and Aeronautical Engineering, University of the Witwatersrand; Johannesburg; South Africa , Hamed.Roohani@wits.ac.za / Nkosinathi.shongwe4@students.wits.ac.za

[2]Department of Mechanical and Industrial Engineering, Ryerson University; Aggrey.Mwesigye@Ryerson.ca

Abstract

Dynamic analysis of a solar powered Ejector Refrigeration System (ERS) is considered under variable solar radiation and weather conditions. A mathematical model representing the performance of the ejector system is developed and implemented in Engineering Equation Solver and further coupled with TRNSYS - transient system simulation tool to determine the solar dependent performance of the system. A comparison of three types of solar collectors shows that Evacuated Tube Collectors (ETC) outperform Photovoltaic-Thermal collectors (PVT) and Photovoltaic (PV) collectors since they give both high COP values and extended cooling hours. PVT and PV-ETC linked systems experience significant thermal energy losses as a result of high collector inlet temperatures which results to the poor performance of the system. Within ETC systems, increasing the storage capacity extends the active cooling period of the system and lowers the generator temperature which results in higher cooling capacity values.

Keywords: Coefficient of Performance; ERS; Evacuated Tube Collectors; Photovoltaic Collectors; Photovoltaic Thermal Collectors

1. Introduction

Space heating and cooling in buildings accounts for a significant amount of energy consumption. About 38% of the total global energy is used in buildings, resulting in about 40% CO2 emissions [1]. In developing countries ,such as South Africa, energy availability is still a challenge which directly affects the economic productivity of the country [2]. Furthermore, most developing countries have high rates of population growth which also adds into the continuously increasing demand for energy, resulting in energy shortages as demand outgrows supply. Moreover, the reliance on fossil fuels for electricity generation has raised concerns as it has been found that the resultant carbon emissions are a major contributor to climate change. Fortunately, the awareness on the detrimental effects of fossil fuel use has gained sufficient momentum in some developing countries which is signified by the use of clean and renewable energy [3].

The energy demand and supply problem is highly coupled to population growth and comfort demands. With the continuous increase in population growth and the subsequent use of high occupancy structures, the demand for space conditioning energy (heating and cooling) is also expected to increase. A sustainable solution to this challenge, especially in locations with abundant solar irradiation, involves the use of solar driven cooling equipment [4].

Numerous studies have been conducted on performance improvement and application of solar cooling systems [5] [6][7]. The ERS forms part of heat driven cooling systems that can be powered from solar thermal energy or other readily available renewable or waste heat. Compared to other solar thermal cooling technologies, the ejector has proven to be the simplest as it does not have any complex moving parts except for a pump. This inherently makes it significantly cheaper than other solar

thermal cooling systems. Another advantage of the ejector is its ability to operate with environmentally friendly working fluids such as water, R1234ze (Z), R1233zd(E), and R600[8][9][10]. The systems ability to operate at low grade thermal heat serves as another advantage of this cycle [11] [12]. The biggest shortcoming of the system has been the low COP values which tend to diminish further when used in a solar thermal application [13].

Several numerical studies have considered the performance of a solar driven ERS under various climatic conditions [14, 15, 16]. These studies have demonstrated the possible use of solar thermal energy to power the ejector.However, such studies have mostly considered constant solar radiance and ambient conditions is not taken into account which nullifies the investigation into the dynamic nature of the system [17, 18, 19]. The current study seeks to determine the dynamic performance of a solar powered ERS by taking into full consideration the variation of both ambient temperatures and solar irradiation. Compared to other fully dynamic studies, this study seeks to achieve optimal operation through the regulation of Generator Temperature (T_g) by having a hot storage reservoir whilst using different solar collectors and maintaining a fixed nozzle geometry [16] [15]. The effect of different solar collectors on the overall performance of the system based on accumulated cooling capacity and active cooling duration, is also investigated. The three types of considered collectors are evacuated tube collectors (ETC), photovoltaic (PV) collectors, and concentrating photovoltaic-thermal (PVT) collectors.

2. Solar Thermal ERS

A solar driven ERS consists of a solar system (used to harvest solar energy) and the ERS which converts the high temperature thermal energy into low temperature cooling energy. From the graphic representation of the system, in Figure 1, it can be seen that the system is made up of three heat exchangers (the generator, condenser, and evaporator). The connection between these heat exchangers is achieved by using the ejector, pump, and throttle valve. During operation, high temperature and pressure working fluid is expanded from the generator through the ejector whereby it entrains the vaporized working fluid exiting the evaporator. The two streams mix and exit the ejector at the condenser pressure whereby heat is rejected and thus transforming the refrigerant to saturated liquid. The liquid is split into the motive stream, which is pumped to the generator, and the secondary stream, which is throttled into the evaporator.

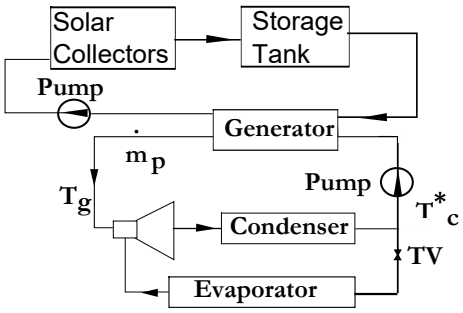

Figure 1: Solar Powered ERS components configuration

Flow analysis through the ejector component is represented in Figure 2.

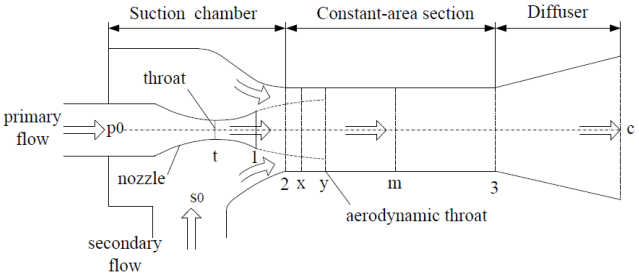

Figure 2: Flow Through the Ejector[20]

Mapping the flow path through the system begins with the entry of the motive flow (hot vaporized refrigerant from the generator) through the converging diverging nozzle whereby it expands to a low pressure in the suction chamber of the ejector. The low pressure region within the suction chamber results in the entrainment of the secondary flow from the evaporator into the ejector. Assuming a constant pressure mixing model, the two streams mix upon attaining the same pressure which is followed by a compression shockwave and pressure regain

process through the diffuser of the ejector. Within this study, the considered solar systems use variable magnitudes of solar thermal and solar electric energy to generate the desired water temperature to vaporize the working fluid across the generator.

3. Model Development

3.1. Ejector Model Development

Modelling the ejector begins with the expansion of the primary fluid through the nozzle after exiting the generator at stagnation pressure (P_{po}) and temperature (T_{po}). These properties are used to evaluate the enthalpy h_{po} and entropy s_{po} at the inlet of the nozzle as indicated in Equation 1.

$$h_{po}, s_{po} = f(T_{po}, P_{po}) \tag{1}$$

These properties are then used to determine the chocked velocity at the throat of the nozzle (v_t) after undergoing an expansion process through the converging section of the nozzle. This is done through an iterative process involving the continuous reduction of (P_t) (the pressure at the throat of the nozzle) which is initially assumed to be equal to (P_{po}). (P_t) is then used to determine the isentropic enthalpy at the throat of nozzle (h_{ts}) which is further used to determine the actual enthalpy (h_t) by considering the expansion efficiency of the nozzle (η_t) as indicated in Equation 2 and Equation 3 respectively.

$$h_{ts} = f(s_{po}, P_t) \tag{2}$$

$$h_t = h_{po} - \eta_t(h_{po} - h_{ts}) \tag{3}$$

The density (ρ_t) and entropy (s_t) at the throat of the nozzle are evaluated so that they can be used together with (P_t) to find the chocked throat velocity (v_t) as shown in Equation 4 and Equation 5 respectively.

$$\rho_t, s_t = f(P_t, h_t) \tag{4}$$

$$v_t = f(P_t, \rho_t) \tag{5}$$

To evaluate the accuracy of (v_t), the enthalpy of the expanded fluid (h'_t) is evaluated again by making use of the nozzle throat velocity as shown in Equation 6.

$$h'_t = h_{po} - (v_t^2/2) \tag{6}$$

This result is compared against previously determined (h_t) and the iterative process is repeated until the two values , (h_t) and (h'_t), are equal. With the final chocked throat velocity known, Equation 7 is used to determine the mass flowrate of the primary fluid (m_p).

$$m_p = \rho_t A_t v_t \tag{7}$$

The exit conditions at the outlet of the nozzle are determined through another iterative process which involves a continuous reduction of the nozzle exit pressure (P_{p1}) which is initially assumed to be equal to (P_t) . This process begins with the evaluation of the nozzle exit density (ρ_{p1}) and nozzle exit enthalpy (h_{p1}), as shown in Equation 8, which are used to evaluate the exit velocity (v_{p1}) and the assumed exit plane enthalpy (h'_{p1}) through Equation 9 and Equation 10.

$$h_{p1}, \rho_{p1} = f(P_{p1}, s_{p1}) \tag{8}$$

$$v_{p1} = m_t/(A_{p1}\rho_{p1}) \tag{9}$$

$$h'_{p1} = h_t + (v_t^2/2) - (v_{p1}^2/2) \tag{10}$$

The iterative process is terminated once h'_{p1} and h_{p1} are equal.

Evaluation of flow properties of the expanded entrained stream in the suction chamber is done an iterative process which involves a continuous reduction of P_{sy} (which is initially equated to P_{so}).

$$h_{sys} = f(P_{sy}, s_{so}) \tag{11}$$

$$h_{sy} = h_{so} - \eta_s(h_{so} - h_{sys}) \tag{12}$$

The inlet stagnation properties (s_{so} and h_{so}) together with the assumed value of P_{sy} and nozzle expansion efficiency (η_s) are used to evaluate the isentropic (h_{sys}) and actual enthalpy (h_{sy}) of the entrained stream as shown in Equation 11 and Equation 12 respectively. h_{sy} and P_{sy} are then used to evaluate the density (ρ_{py}), entropy (s_{so}) and velocity (v_{sy}) of the chocked secondary stream.

To verify the accuracy of v_{sy}, the chocked enthalpy of the secondary stream is re-evaluated as shown in Equation 12.

$$h'_{sy} = h_{so} - (v_{sy}^2/2) \tag{13}$$

The iterative process is terminated once the difference between h'_{sy} and h_{sy} is minimal. Based on the

constant pressure mixing assumption, the pressure of the mixed flow stream P_m is set to be equal to the final expanded pressure of the entrained stream (P_{sy}) which is also equal to the expanded primary flow pressure at section y, (P_{py}). These properties are then used for evaluating the expanded primary flow properties which include the density (ρ_{py}), isentropic enthalpy (h_{pys}), actual enthalpy ((h_{py})) , and expanded primary velocity (v_{py}) as shown in Equation 14, Equation 15, and Equation 16.

$$h_{pys}, \rho_{py} = f(P_{py}, S_{py}) \tag{14}$$

$$h_{py} = h_{p1} - \eta_m(h_{p1} - h_{pys}) \tag{15}$$

$$v_{py} = \sqrt{(2(h_{p1} + (v_{p1})^2/2) - h_{py})} \tag{16}$$

To evaluate the entrained mass flow-rate (m_s), Equation 17 is used whereby the cross sectional area of the secondary fluid at section y (A_{sy}) and the cross sectional area of the primary fluid at section y (A_{py}) are evaluated from Equation 18 and,Equation 19 respectively.

$$m_s = \rho_{sy} A_{sy} v_{sy} \tag{17}$$

$$A_{sy} = A_3 - A_{py} \tag{18}$$

$$A_{py} = m_p/(\phi_m v_{py}) \tag{19}$$

The energy and momentum balance of the two streams (primary and secondary) and the resultant mixed stream is shown in Equation 23 and Equation 24 with (h_m) , (v_m), and (ϕ_m) being the mixed stream enthalpy, mixed flow velocity , and mixing efficiency ,respectively.

$$Primary = m_p(h_{py} + ((v_{py})^2/2)) \tag{20}$$

$$Secondary = m_s(h_{sy} + ((v_{sy})^2/2)) \tag{21}$$

$$Mixed = (m_p + m_s)(h_m + ((v_m^2)/2)) \tag{22}$$

$$Primary + Secondary = Mixed \tag{23}$$

$$\phi_m(m_p v_{py} + m_s v_{sy}) = (m_p + m_s) v_m \tag{24}$$

The compression shock process is also modelled through another iterative procedure which involves making continuous increments on the aftershock density (ρ_3) of flow from the initially assumed value of (ρ_m). The assumed aftershock density is used to evaluate the aftershock pressure (P_3) as indicated in Equation 26.

$$P_3 = P_m + (\rho_3 - \rho_m)(\rho_3/\rho_m) v_m^2 \tag{25}$$

The accuracy of (P_3) is ensured by minimizing the difference between (h_3) and (h_3') which are evaluated in Equation 26 and Equation 27, respectively.

$$s_3, h_3 = f(P_3, \rho_3) \tag{26}$$

$$h_3' = h_m + ((P_3 - P_m)/2)((\rho_(m) + \rho_m)/\rho_m \rho_3) \tag{27}$$

With the aftershock conditions known, fluid pressure recovery across the diffuser is modelled as shown in Equation 28 to Equation 31.

$$h_{cc} = h_3 + (v_3^2/2) \tag{28}$$

$$v_3 = \sqrt{(2(h_m + (v_m)^2/2) - h_3)} \tag{29}$$

$$h_{cs} = h_3 + \eta_d(h_{cc} - h_3) \tag{30}$$

$$P_{cc} = P_{cs} = f(h_{cs}, s_3) \tag{31}$$

In sub-critical mode, expansion of primary flow does not generate sufficient suction pressure to result in full expansion of the secondary stream. Due to the poor expansion of the primary flow, which only reaches section x compared to the much further section y (graphically presented in **??**), its expanded pressure (P_{px}) is assumed to be equal to (P_{so}) whilst the entropy at this section (s_{px}) is equal to that at the exit plane of the nozzle (s_{p1}). Using the nozzle exit conditions and enthalpy at section x (Equation 32) ,Equation 29, the velocity of the primary flow at section x (v_{px}) is calculated as shown in Equation 33.

$$h_{px} = f(P_{px}, s_{px}) \tag{32}$$

$$v_{px} = \sqrt{(2(h_{p1} + (v_{p1})^2/2) - h_{px})} \tag{33}$$

The evaluation of sub-critical performance of the ejector is done by establishing the condenser break down pressure Critical Break Down Pressure (P_{cb}) (P_{cb}) which is used together with the actual condenser pressure (P_c) and critical condenser pressure (P_{cc}) to ascertain the fractional adjustment of the critical entrainment ratio (u_c) as shown in Equation 34.

$$u = u_c(P_{cb} - P_c)/(P_{cb} - P_{cc}) \tag{34}$$

At the break down point, there is minimal entrainment of the secondary stream. To consider the effect of the secondary stream on P_{cb}, the entrained secondary flow-rate (m_{sx}) is set to a small value of 1e−6 kg/s and v_{sx} is evaluated based on the flow density. Equation 13, Equation 23 ,and

Equation 24 are used to evaluate h_{sx} , h_m, and v_m with h_{py}, v_{py} , h_{sy} , ϕ_m ,and η_t, v_{sy} being replaced by h_{px} , v_{px} , h_{sx}, ϕ_{mb} ,andv_{sx} respectively. The mixed flow properties are further used to assess aftershock properties of the flow through the use of Equation 26- Equation 27. The ejector break down pressure P_{cb} is evaluated from Equation 28 - Equation 31 through the substation of h_{cc} and P_{cc} with h_{cb} and P_{cb}, respectively. The Coefficient of Performance (COP) of the ERS is evaluated according to Equation 35.

$$COP = \frac{Cooling\ Capacity}{Generator\ Heat\ Input} \tag{35}$$

3.2. TRNSYS Model Development

The configuration and performance evaluation of the three solar energy harvesting systems is undertaken in TRNSYS [19].

3.2.1 ETC Powered ERS

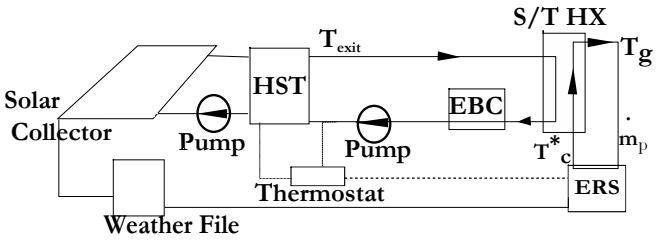

Figure 3: A schematic of an ETC powered ERS

This system makes use of ETC (TYPE71) for converting solar irradiation to thermal energy which is transferred to the working fluid. The working fluid is circulated by a pump (TYPE3b) from the collector to the thermally stratified storage tank (TYPE4a). The boiling point of the tank is limited to 80 ℃in order to limit excessively high T_g values which then cause low COP values. To guarantee positive thermal energy gain across the collectors, the pump is controlled by a timer (TYPE14h) which allows flow circulation between 7 AM 16 PM. The working fluid is circulated to the generator (modelled as a TYPE5g heat exchanger) of the ejector by another TYPE3b pump. Operation of this pump is based on the output of a 5 stage thermostat (TYPE108) which monitors the top node temperature of the storage tank and allows flow circulation once it is above 65 C. Upon reaching this condition, the thermostat simultaneously sends another signal to activate the ejector (modelled as a TYPE42a component).

Solar and weather data is accessed through a TYPE15 component and is used by the collectors and the ejector for determining the Condenser Temperature (T_c). Presented in a graphic format is the configuration of the above stated components in Figure 3 with the specifications listed in Table 1.

Component	**TRNSYS Label**	**Specifications**
ETC	Type71	Area: 10 m^2 - 70 m^2
Thermostat	Type108	Set Temperature =65 ℃
$Pump_{Collector}$	Type3b	Rated = 1500 kg /hr
Storage Tank	Type4a	Volume = 2.33 m^3 Boiling Point = 80℃
Pump	Type3b	Rated = 1200 kg /hr
Calculator		Energy Balance Calculator
S/T HX	Type5g	Works as the generator. UA_{HX} = 5400 kJ/hr_K
Weather Data	Type15	Location: Johannesburg
Ejector	Type42a	Imports the performance data of the component

Table 1: ETC Powered ERS Component Specifications

3.2.2 PV and ETC Powered ERS

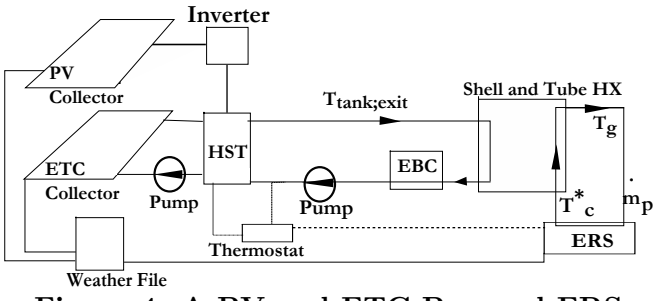

Figure 4: A PV and ETC Powered ERS

This system seeks to exploit the benefits of both forms of solar (PV and thermal) energy. A graphic representation of the system is shown in Figure 4. The specification of the solar system components is conducted in a parametric analysis motivated by determining optimal performance. To ensure that instant power is available for system start up, a grid-tied version of the system is considered whereby

electricity can be drawn from the grid to supplement excess power requirements. The role of the PV array is to generate enough electricity to replace any grid utilised supply.

Compo -nent	**TRNSYS Label**	**Specifications**
PV array	Type194	PV area: $9-30m^2$
Inverter	Type48a	Inverter $\eta = 91\%$ [1]

Table 2: TRNSYS Specifications of PV array and Inverter

Table 2 shows the specification of PV panels and the inverter as sourced from the study conducted by Quesada et al [1].

3.2.4 Concentrating PVT Powered ERS

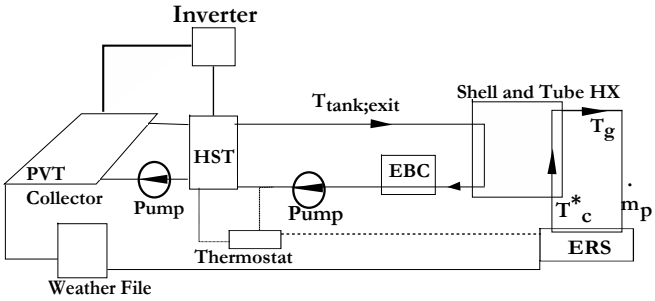

Figure 5: A PVT powered ERS

With the goal of exploiting both solar thermal and solar electric energy, the performance of PVT collectors in powering the ERS is also considered. The system layout is shown in Figure 5 with the specifications in Table 3.

Component	**TRNSYS Label**	**PV Area**
PVT array	Type50e	$100m^2 - 150m^2$

Table 3: PVT Array Specification

4. Models Validation

4.1 Validation of EES model.

To validate the ERS model developed in the current study, results from Li et. al. [20] are used to compare the Critical Condenser Pressure (P_{cc}) and entrainment ratio (U_c) at different operating conditions (T_g and Evaporator Temperature (T_e)) and at different Ejector Area Ratio (EAR). From the results shown in Table 4, it is evident that the ejector model developed in the current study accurately regenerates the results from [20].

EAR	T_g	T_e	[20]	Model	[20]	Model
-	-	-	P_{cc}	P_{cc}	U_c	U_c
-	[°C]	[°C]	[kPa]	[kPa]	[-]	[-]
2,77	75	12,5	0,92	0,92	0,11	0,11
3,32	75	12,5	0,87	0,87	0,23	0,23
3,32	80	12,5	0,93	0,93	0,17	0,17
3,32	85	12,5	0,99	0,99	0,12	0,12
3,96	75	12,5	0,82	0,82	0,37	0,37
3,96	80	12,5	0,88	0,88	0,30	0,30
3,96	85	12,5	0,94	0,94	0,23	0,23

Table 4: Validation of R134a Ejector model

4.2 Validation of TRNSYS PV Model

The PV model developed in the current study is validated by comparing the monthly energy outputs against the results published in Quesada et al[1]. The PV model is set to have the same inputs, weather data and component specifications, as extracted from the publication. From Table 5, it is evident that the present PV predicts the performance of the published model with a maximum deviation in results of about 11.67% whilst the common deviation is less than 6%.

Month	Monthly PV output kWh	Present Model kWh	% Deviation
January	500	482	3,6
February	685	765	11,67883
March	950	896	5,684211
April	1067	1009	5,435801

Table 5: Validation of PV system

4.3 Validation of TRNSYS ETC Model

The ETC model is validated from the results published by Tashtoush et al [13]. The outcome of the validation is shown in Table 6 from which it is evident that the maximum deviation (Δ) at the different solar collector areas is 8,3 %.

Collector Area m^2	Annual Useful Energy kW.h	Annual Useful Gain kW.h	Δ %
10	25000	24500	2
40	112500	103162,5	8,3
90	200000	194000	3

Table 6: Validation of ETC system

4.2 Validation of TRNSYS PVT Model

The PVT model is validated from the results published in Kalogirou [21]. Table 7 shows that the maximum deviation of the results generated in the current study is 6% and 5% for both electric and thermal energy output of the PVT system, respectively.

Water $\dot{m}$ L/hr	Electric Output GJ [21]	Present Model GJ	Thermal Output GJ [21]	Present Model GJ
0	0,977	0,957	0	0
20	2,584	2,429	6,721	6,697
25	2,646	2,588	8,293	7,878
50	2,737	2,721	4,308	4,157

Table 7: Validation of PVT model

5. Results

4.1 ETC System Performance

The effect of the collector area on the system's Evaporator Cooling Capacity ($\dot{Q}_{cool}$) is shown in Figure 6. In all of the considered plots, the typical operation characteristics of a fixed geometry ERS is evident. Figure 6 shows that as the day progresses, both COP and $\dot{Q}_{cool}$ decrease due to increments of T_g and T_c. The drop in COP and $\dot{Q}_{cool}$ stops once T_g reaches the storage tank limit temperature of 80 ℃. As the availability of solar radiation diminishes with time, the system regains $\dot{Q}_{cool}$ and COP values due to lower T_g and T_c. The results indicate that as the collector area increases, the system is able to function for durations extending beyond the availability of solar irradiation. This is clearly seen on the performance of the 10 m^2 collector area which stops operating at 15:45 due to the low storage tank temperature to load. Increasing the collector area from 10 to 25 m^2 increase the stop time to 21:08 whilst 40 m^2 , 55 m^2 , and 70 m^2 increases the stop time to 21:23 , 21:30, and 21:30, respectively.

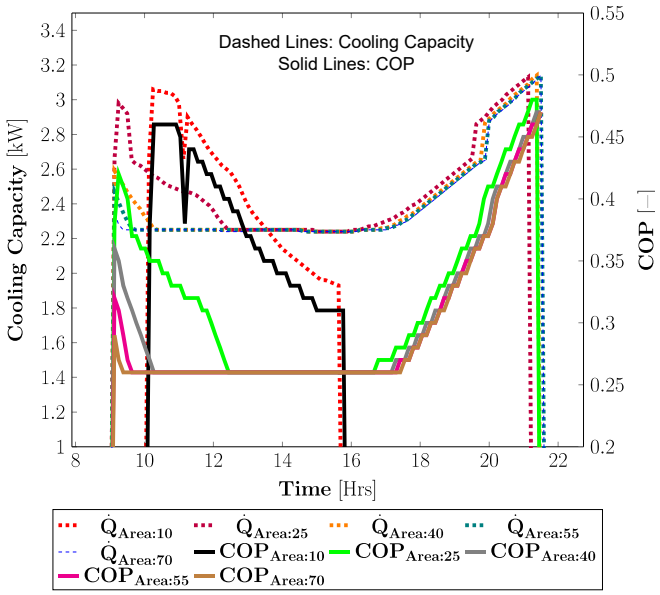

Figure 6: ETC powered ERS at variable collector areas

Figure 6 shows that as the systems active operation period increases, the cooling capacity of the system decreases with the daily accumulated cooling capacities at different areas being 113.16 kW ($10m^2$), 243.10 kW (25 m^2), 241.37 kW (40 m^2), 242.60 kW (55 m^2), and 241.84 kW (70 m^2). This comes as the result of high generator temperatures experienced at larger collector areas which results in a decrease in the performance of the ERS. This is evident when considering the performance of the 10 m^2 system which is seen to achieve the highest cooling capacity and COP during its active operation period whilst simultaneously operating at the lowest generator temperature of 65 ℃. The high cooling capacity coupled with the low generator temperature inherently results in high COP values (also shown in Figure 6). However, due to the small collector area, the 10 m^2 system experiences a startup delay because of the slow rate of thermal energy harvesting. This is clearly not a problem with collector areas above 10 m^2 as Figure 6 shows that they all start at 9:00 AM.

From Figure 7 it can be seen that T_g remains constant, as a result of the fixed boiling point temperature of the storage tank, whilst the magnitude of harvested thermal energy varies according to the available solar radiation.

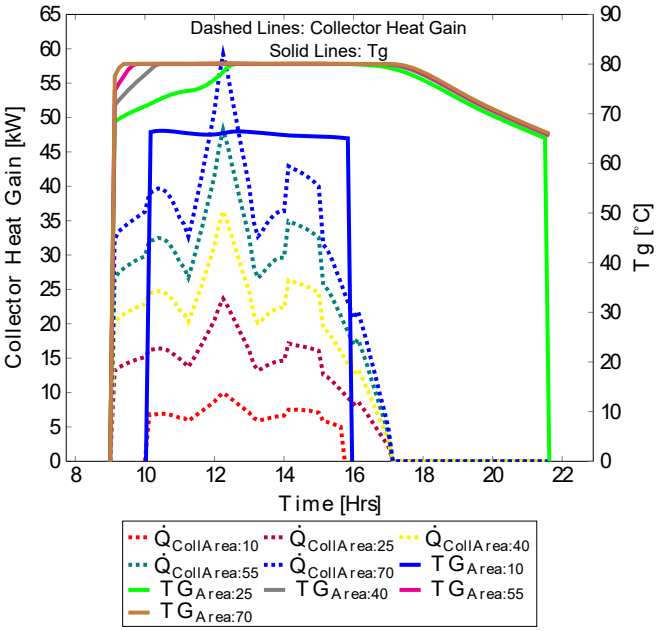

Figure 7: Effect of collector heat gain on T_g

However, the stable T_g value does not provide sufficient isolation of the system from its operating environment as the increase and decrease of T_c results in a decrease (during the morning) and increase (during the afternoon) in the cooling capacity of the system. Figure 7 shows that increasing the collector area results in the expected outcome of increasing the amount of harvested solar thermal energy which subsequently results in extended active cooling hours. With the plots in Figure 7, it is concluded that the optimal collector area is 25 m^2 as it is the smallest area to achieve the same cooling hours as delivered by larger collector areas.

4.2 Hybrid (PV with ETC) Ejector Powered Refrigeration System

Analysis of this system is undertaken through the variation of the ETC area to determine the electric energy required to achieve the target T_g. Figure 8 shows that increasing the ETC area results in the anticipated outcome of reducing the electric requirement of the hybrid system. Due to the availability of instant electricity for heating water within the tanks, in all cases, the system starts instantly at 8:00. However, the stop time is dependent on the amount of thermal energy stored within the tanks. The largest ETC area (10 m^2) and second largest ETC area (8 m^2) , operate for the same duration (8:00 to 21:00) with the second largest collector area generating higher COP values between the two.

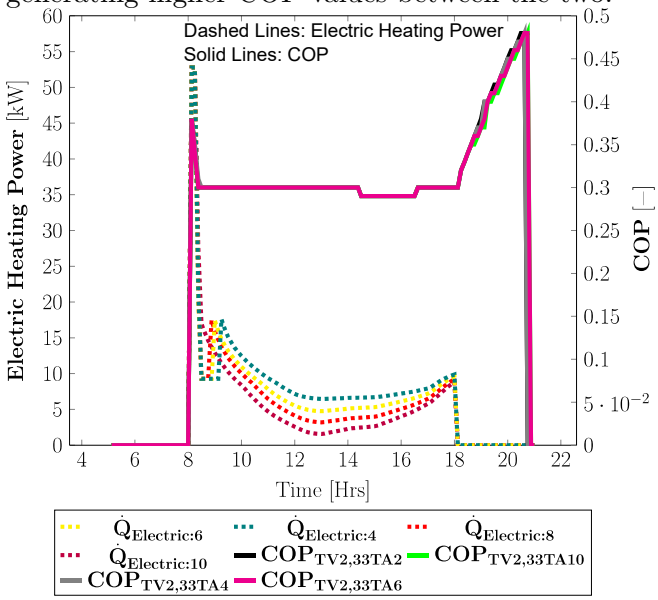

Figure 8: PV and ETC powered ERS performance under variable ETC areas

ETC areas of 4 m^2 and 6 m^2 simultaneously stop at 20:45 and of these systems, the 4 m^2 ETC area achieves the highest COP values. The results are in perfect alignment with the basic principles of the ERS as higher thermal energy intensity is expected to result in higher generator temperature values which reduces COP values. It can also be noted that the electric heating requirement is inversely proportional to the amount of solar thermal energy available during the day.

Figure 9 investigates the effect of a larger storage tank (4.62 m^3) on the amount of electricity consumed and on the amount of thermal energy harvested. Comparing Figure 8 against Figure 9, it is evident that increasing the size of the storage tank results in extended hours of operation. The effect of the ETC area on the demand of electric energy required by the system is shown in Figure 10. From the plots it is evident that increasing the ETC area

from 4 m^2 to 8 m^2 (whilst the PV area is constant) results in a significant drop in the demand of electric energy. This is an expected outcome since larger ETC area means higher thermal energy gains across the collector which also means less electric energy demand to generate the desired water temperature. With the availability of both electric (PV) and thermal (ETC) energy, increasing PV surface area only reduces the amount of grid drawn electricity but does not result in significantly extended active cooling hours as there is minimal thermal energy accumulation at low T_g temperatures.

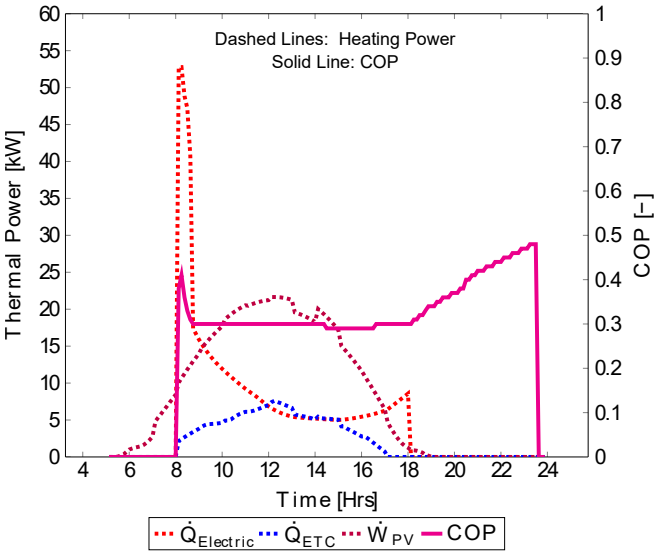

Figure 9: Effect of storage capacity on the performance of a PV and ETC ejector

With PV dominant cooling systems, accumulative thermal energy storage can be achieved by raising the storage tank limit temperature above 77 ℃. However, the COP of the ERS drops as a result of high T_g values. Figure 10 also shows the variation of PV generated electricity with the number of PV panels in series.

4.3 Hybrid (PVT) Ejector Powered Refrigeration System

Figure 11 shows the performance of a PVT collector when supplying thermal and electric energy to the ERS. The plots show that the minimum collector area which results in zero net electric grid demand of the system is 150 m^2 . At 150 m^2 , the PVT system is able to cater to all of the systems electric requirements and generates an additional 104 kW whilst the 125 m^2 collector area system requires an additional 29 kW. The impact of solar thermal energy in the system is evident when noting that the system stops demanding electric energy input at the same time water starts flowing into the collectors. Water flow into the collectors is delayed to start at 10:00 in-order to ensure that the collectors will add thermal energy into the water flowing in from the tank.

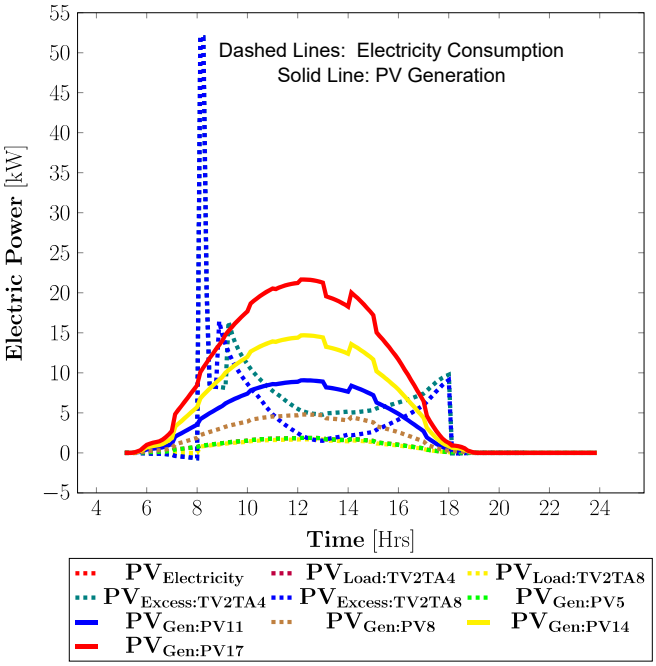

Figure 10: Analysis of ETC and PV area on system performance

An hourly analysis of the system, as plotted in Figure 11, shows the large magnitude of electric power ($\dot{W}_{excess;150}$) required by the system as indicated by the 48 kW spike in the excess electricity plot. Thereafter, the requirement of grid supplied electricity gradually decreases as the PV panels start generating power ($\dot{W}_{PV;150}$) with the availability of solar irradiation. At peak solar radiation periods (10:00 to 15:00), the thermal energy from the collectors ($\dot{Q}_{Thermal;150}$) is sufficient for maintaining T_g above 77 ℃ which eliminates the demand for any electric energy and hence resulting in electricity transfer to the grid. Figure 12 shows

that a PVT driven system fails to provide sufficient thermal storage to enable extended hours of operation beyond sunset. This is because the system's thermal reservoir is predominantly generated from electric energy which is used to raise the water temperature to the minimum generator temperature required.

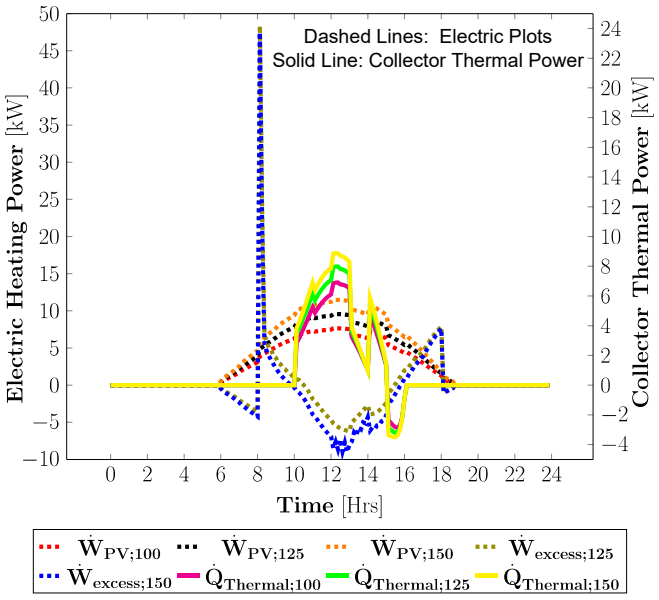

Figure 11: Electric and thermal performance of a PVT powered ejector

Utility of solar thermal energy is limited for periods with high solar irradiation (10:00 to 16:00) in order to avoid heat losses within the collector.

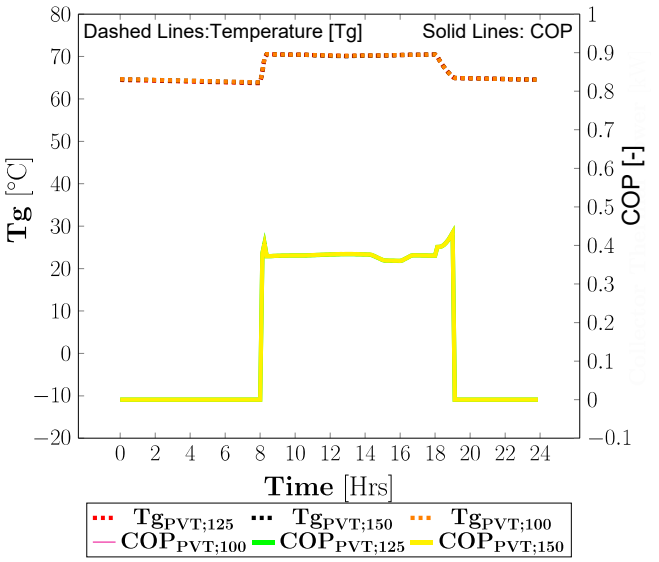

Figure 12: Performance of a PVT powered ejector cycle

5. Conclusion

In this study, a dynamic analysis of a solar powered ERS has been undertaken using the climatic conditions in Johannesburg. The study shows that using large surface area ETC is the most effective method of supplying solar thermal energy. Using both solar thermal and solar electric energy in a single tank system results significant useful heat losses through the collectors. This challenge suggests further system optimization through implementation of separate tanks for separately harvesting electric and thermal energy whereby thermal stratification within the solar thermal tank would ensure relatively low collector inlet temperatures. The results also show that in order to attain active cooling beyond the availability of solar radiation, a large storage tank is desirable since it provides sufficient thermal stratification which results in continuous heat harvesting during the day. However, the results also show that if desired, supreme cooling capacity without extended hours of operation can be obtained when a 10 m^2 collector area is used.

Acknowledgements

The authors acknowledge funding from the National Research Fund (NRF).

References

[1] B. Quesada, C. Snchez, J. Caada, R. Royo, and J. Pay, "Experimental results and simulation with trnsys of a 7.2kwp grid-connected photovoltaic system," *Applied Energy*, vol. 88, no. 5, pp. 1772 – 1783, 2011.

[2] H. Joffe, "Challenges for south africas electricity supply industry," *The Journal of the Helen Suzman Foundation*, pp. 33–37, February 2012.

[3] P. Gauché, T. W. von Backström, and A. C. Brent, "A concentrating solar power value proposition for South Africa," *Journal of Energy in Southern Africa*, vol. 24, pp. 00 – 00, 01 2013.

[4] P. Kohlenbach and U. Jakob, *Solar Cooling: The Earthscan Expert Guide to Solar Cooling Systems*, ser. Earthscan Expert. Taylor & Francis, 2014.

[5] A. Allouhi, T. Kousksou, A. Jamil, P. Bruel, Y. Mourad, and Y. Zeraouli, "Solar driven cooling systems: An updated review," *Renewable and Sustainable Energy Reviews*, vol. 44, pp. 159 – 181, 2015.

[6] T. Ge, R. Wang, Z. Xu, Q. Pan, S. Du, X. Chen, T. Ma, X. Wu, X. Sun, and J. Chen, "Solar heating and cooling: Present and future development," *Renewable Energy*, pp. –, 2017.

[7] T. Otanicar, R. A. Taylor, and P. E. Phelan, "Prospects for solar cooling an economic and environmental assessment," *Solar Energy*, vol. 86, no. 5, pp. 1287 – 1299, 2012.

[8] A. Mwesigye and S. B. Dworkin, "Performance analysis and optimization of an ejector refrigeration system using alternative working fluids under critical and subcritical operation modes," *Energy Conversion and Management*, vol. 176, pp. 209 – 226, 2018.

[9] V. Nguyen, S. Riffat, and P. Doherty, "Development of a solar-powered passive ejector cooling system," *Applied Thermal Engineering*, vol. 21, no. 2, pp. 157 – 168, 2001.

[10] B. Saleh, "Performance analysis and working fluid selection for ejector refrigeration cycle," *Applied Thermal Engineering*, vol. 107, 2016.

[11] R. Yapıcı and F. Akkurt, "Experimental investigation on ejector cooling system performance at low generator temperatures and a preliminary study on solar energy," *Journal of Mechanical Science and Technology*, vol. 26, no. 11, pp. 3653–3659, Nov 2012.

[12] Y. Xu, N. Jiang, Q. Wang, X. Han, Z. Gao, and G. Chen, "Proposal and thermodynamic analysis of an ejectioncompression refrigeration cycle driven by low-grade heat," *Energy Conversion and Management*, vol. 145, pp. 343 – 352, 2017.

[13] B. Tashtoush, A. Alshare, and S. Al-Rifai, "Hourly dynamic simulation of solar ejector cooling system using trnsys for jordanian climate," *Energy Conversion and Management*, vol. 100, pp. 288 – 299, 2015.

[14] W. Pridasawas and P. Lundqvist, "A year-round dynamic simulation of a solar-driven ejector refrigeration system with iso-butane as a refrigerant," *International Journal of Refrigeration*, vol. 30, no. 5, pp. 840 – 850, 2007.

[15] Y. Allouche, S. Varga, C. Bouden, and A. C. Oliveira, "Dynamic simulation of an integrated solar-driven ejector based air conditioning system with pcm cold storage," *Applied Energy*, vol. 190, no. Supplement C, pp. 600 – 611, 2017.

[16] M. Dennis and K. Garzoli, "Use of variable geometry ejector with cold store to achieve high

solar fraction for solar cooling," *International Journal of Refrigeration*, vol. 34, no. 7, pp. 1626 – 1632, 2011, ejector Technology.

[17] B. Huang, J. Chang, V. Petrenko, and K. Zhuk, "A solar ejector cooling system using refrigerant r141b," *Solar Energy*, vol. 64, no. 46, pp. 223 – 226, 1998.

[18] H. Vidal, S. Colle, and G. dos Santos Pereira, "Modelling and hourly simulation of a solar ejector cooling system," *Applied Thermal Engineering*, vol. 26, no. 7, pp. 663 – 672, 2006.

[19] G. Alexis and E. Karayiannis, "A solar ejector cooling system using refrigerant {R134a} in the athens area," *Renewable Energy*, vol. 30, no. 9, pp. 1457 – 1469, 2005.

[20] F. Li, Z. Chang, Q. Tian, C. Wu, and X. Wang, "Performance predictions of dry and wet vapors ejectors over entire operational range," *Energies*, vol. 10, no. 7, 2017.

[21] S. A. Kalogirou, "Use of trnsys for modelling and simulation of a hybrid pvthermal solar system for cyprus," *Renewable Energy*, vol. 23, no. 2, pp. 247 – 260, 2001.